ACS APPLIED MATERIALS & INTERFACES

www.acsami.org

Research Article

Hyaluronan Brush-like Copolymers Promote CD44 Declustering in Breast Cancer Cells

Ana M. Carvalho, Jesus Valcarcel, Diana Soares da Costa, Marisa Gomes, José Antonio Vázquez, Rui L. Reis, Ramon Novoa-Carballal,* and Iva Pashkuleva*

Cite This: https://doi.org/10.1021/acsami.2c11864

Read Online

ACCESS | Metrics & More | Article Recommendations | Supporting Information

ABSTRACT: We report on the synthesis of hyaluronan (HA) brush-like copolymers and their application as antagonists of tumorigenic CD44-HA interactions. HA (4.8 kDa, ca. 24 saccharides) was grafted on 2-hydrohyethyl methacrylate (HEMA) by end-on oxime ligation. The obtained copolymers were compared with low and high molecular weight HA in terms of hydrolysis kinetics in the presence of hyaluronidase (isothermal titration calorimetry) and interactions with CD44 (surface plasmon resonance). The results evidenced that the high molecular weight HA and HA-*g*-HEMA have a much higher affinity to CD44 than low molecular weight HA. Additionally, slower enzymatic degradation was observed for the copolymer, making it an excellent candidate for active targeting of tumorigenic CD44-HA interactions. We, therefore, investigated the effect of the copolymer on cancer cell lines with different expression of CD44 and observed an efficient declustering of CD44 that is usually associated with reduction of metastasis and drug resistance.

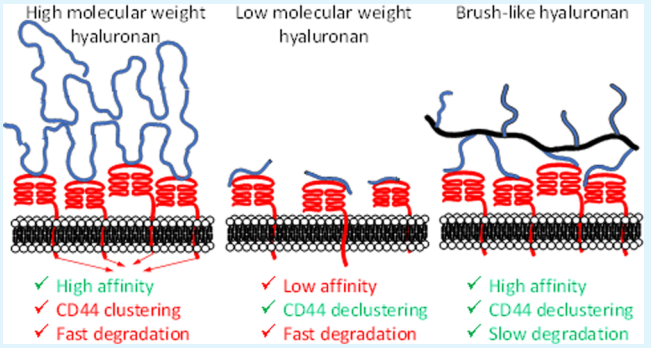

KEYWORDS: *hyaluronic acid, end-on modification, oxime ligation, hyaluronidase, isothermal titration calorimetry, surface plasmon resonance, cancer therapy, CD44 antagonist*

1. INTRODUCTION

Hyaluronan (HA) is a linear, nonsulfated glycosaminoglycan (GAG) composed of a repeating disaccharide β(1,4)-D-glucuronic acid-β(1,3)-*N*-acetyl-D-glucosamine (Figure 1A).[1,2] It is synthesized at the cell membrane by HA synthases and continually secreted in the pericellular and extracellular space as a high molecular weight polymer (HMW, above 1000 kDa, Figure 1B (**1**)). These long chains are then fragmented to low molecular weight HA (LMW, 1 to 500 kDa, Figure 1B (**2**)) by the action of hyaluronidases (HYALs) and reactive oxygen and nitrogen species.[2,3]

The diverse biological functions of HA are related to the wide variety of sizes of this GAG.[1−4] In cancer, for example, HA metabolism and catabolism are commonly deregulated, leading to the accumulation of either HMW or LMW forms within the tumor microenvironment.[1,2,5−7] HMW HAs form a functional pericellular coat by organization and clustering of several extracellular and membrane proteins (including CD44, Figure 1C), growth factors, and cytokines via multivalent interactions.[1,2,8,9] This coat provides sustained activation of antiapoptotic, pro-invasion, and migration signaling pathways that facilitate the intravasation, protect against anoikis during circulation, and contribute to ectopic tissue colonization.[1,2,9−12] It also promotes the translocation of proteins and monocarboxylate transporters to the cell membrane that increase multidrug resistance and cancer cell survival.[13−15] On the other hand, LMW HA fragments can attenuate the effects of HMW HA by competitive binding to the main HA receptor CD44: binding of LMW HA to CD44 disrupts the CD44 clusters that are formed in the presence of HMW HA (Figure 1C). This process, known as CD44 declustering, leads to inhibition of pro-tumorigenic signaling responses.[1,2,16,17]

HA oligosaccharides (6−15 saccharides) have been used to reduce the aggressiveness and metastatic potential of tumor cells and augment the responsiveness to the currently used chemotherapies.[18,19] The therapeutic use of HA oligosaccharides, however, has some drawbacks: several studies have reported that these fragments can also activate pathways toward cell migration, inflammation, and proliferation related with the metastasis as well as challenging targeted delivery *in vivo* given the oligosaccharides susceptibility to degradation by the overexpressed HYALs to shorter fragments that do not bind CD44.[20,21] Thus, several other strategies that target the

Received: July 4, 2022
Accepted: August 24, 2022

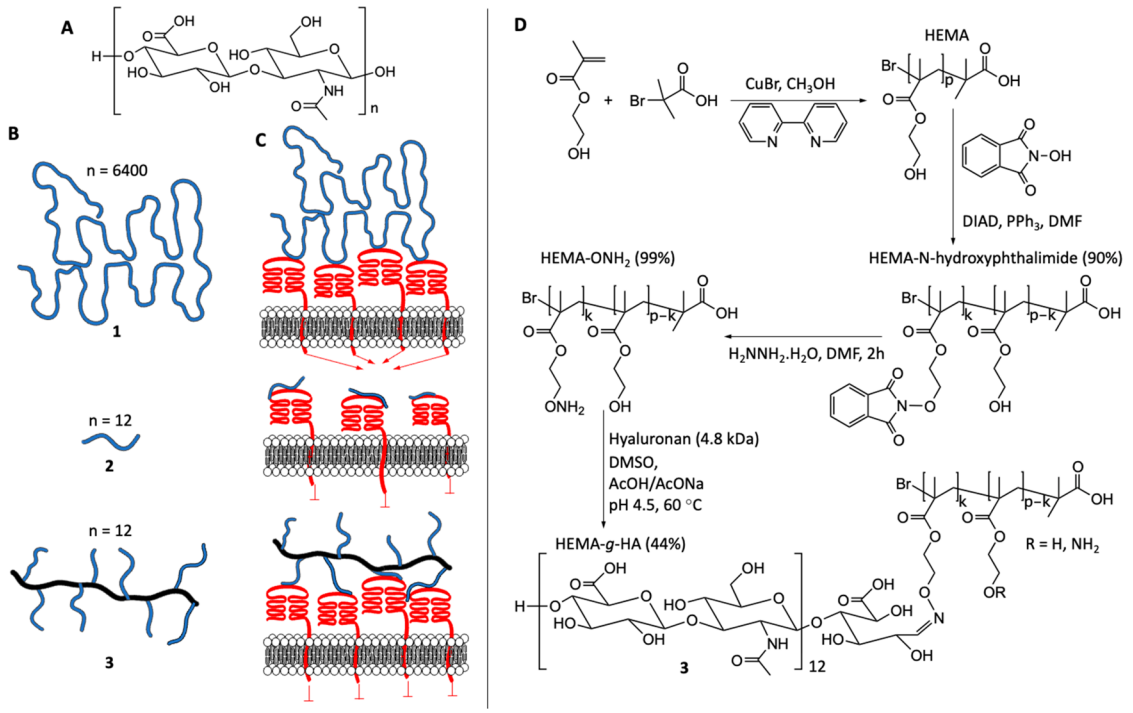

Figure 1. Schematic presentation of the polymers used in this study and their interactions with CD44 receptors: (A) Chemical structure of the repeating disaccharide unit of hyaluronan (HA). (B) Cartoon representation of high molecular weight HA (**1**, 1.35 MDa), low molecular weight HA (**2**, 4.8 kDa), and HA-brush like copolymers HEMA-*g*-HA (**3**, each HA branch is 4.8 kDa). (C) Their mode of binding to CD44 receptors and (D) synthetic pathway used for the preparation of hyaluronan brush-like copolymers (**3**, HA-*g*-HEMA).

interactions between HMW HA/CD44 and CD44 declustering have been explored, such as the addition of soluble CD44[22] or peptides with HA-binding motifs[23] to bind the endogenous HMW HA; blocking cancer-specific CD44 variants (CD44v) with antibodies[24,25] or function inhibitory peptides;[26−30] and deletion of CD44v using siRNA/shRNA.[31] Herein, we propose an alternative simple and cost-effective strategy that uses a brush-like glycopolymer of HA (Figure 1B, **3**). This copolymer has several LMW HA branches that bind CD44 in a multivalent fashion, thus, ensuring high affinity to this receptor (Figure 1C). Its interactions with CD44 are, however, different from the HMW HA-CD44 binding as they do not induce CD44 clustering. On the contrary, when used in a competitive assay with endogenous HA, the copolymer induced CD44 declustering.

2. MATERIALS AND METHODS

2.1. Materials. All reagents were purchased from Sigma-Aldrich if not specified. Aniline was purified by distillation under a vacuum. The other reagents were used without further purification. Sodium hyaluronate (HA, average molecular weight of 4.8 kDa and 1.35 MDa) was obtained from Lifecore Biomedical LLC (USA). These molecular weights were chosen based on previous data for bioactivity of low and high molecular weight HA,[1−9] as well as on our previous experience.[4,32−35] The antibodies used in this study were monoclonal antibody to CD44-Ascites (Acris) and AlexaFluor 594 donkey antimouse IgG1 (H+L). We used 4′,6-diamidino-2-phenylindole (DAPI, Biotium) and fluorescein isothiocyanate labeled phalloidin (phalloidin-FITC). Ultrafiltration and dialysis membranes (Millipore) from regenerated cellulose with cut-offs of 1, 3, 5, 12 and 30 kDa were used.

2.2. Polymerization of 2-Hydroxyethyl Methacrylate (HEMA). We used atom transfer radical polymerization (ATRP) with an alkyl bromoinitiator and CuBr/2,2′-bipyridine as a catalyst.[36] HEMA (99%, Aldrich) was passed through a plastic syringe filled with basic alumina to remove the inhibitor. A round-bottom flask was charged with 2-bromo-2-methylpropionic acid (0.12 g, 1 equiv), HEMA (20 g, 220 equiv), 2,2′-bipyridine (1.1 g, 10 equiv), and 5 mL of methanol. The mixture was degassed with a N_2 stream, and CuBr (0.5 g, 5 equiv) was added into the reaction system under N_2. Next, the polymerization was performed at 40 °C for 24 h under magnetic stirring. The reaction flask was opened and bubbled with air to stop the polymerization. The crude reaction product was dissolved in methylene chloride, and the solution passed through a column with neutral aluminum oxide to remove the copper catalyst and dialyzed (M_w cut off 12 kDa, cellulose) against ethanol to remove the excess of the monomer. After 7 days of dialysis, water was added, ethanol was evaporated under vacuum, and the polymer was recovered by lyophilization. The polymer prepared was analyzed by NMR (d-DMSO) and GPC.

2.3. Synthesis of HEMA-ONH$_2$. Poly-HEMA (1 equiv),*N*-hydroxyphthalimide (*N*-Pht, from 0.5 to 1.2 equiv with respect to OH of HEMA to obtain different degrees of substitution), and triphenylphosphine (same equivalents as N-Pht) were mixed in dried DMF (ca. 20 g/L mL of HEMA) under N_2 atmosphere. To this mixture diisopropyl azodicarboxylate (same eq as N-Pht) was added dropwise (color change to red). The reaction was stirred at room temperature for 24 h. The product was purified by ultrafiltration (cut off 5 kDa) in DMF. An excess of water was added, and freeze-drying was performed. The obtained products were analyzed by NMR. The degree of substitution (DS) was determined by integration of the peaks corresponding to the phthalimide substituted −OH groups and was found to be 10, 25, 50, 60, 80, and 100%. The phthalimide group was cleaved by the addition of hydrazine hydrate (3 equiv per phthalimide group) in DMF, leading to the deprotected aminooxy group. After 2 h, the product was diluted in water and freeze-dried under a vacuum. The cleavage was confirmed by NMR. The crude product was used in the next step without further purification or alternatively ultrafiltered in DMF (details in the Supporting Information) with a cellulose membrane (cut off 5 kDa).

2.4. Synthesis of HEMA-*g*-HA (3). The reaction conditions (excess of HA, cosolvent ratio, reaction time, temperature, and

https://doi.org/10.1021/acsami.2c11864
ACS Appl. Mater. Interfaces XXXX, XXX, XXX−XXX

catalyst) were optimized for the oxime condensation between HEMA-ONH_2 and LMW HA (**2**) (Table S1). The crude HEMA-ONH_2 and the respective amount of HA were mixed in an acetate buffer (AcOH/AcONa; 0.078 M AcOH/0.0625 M AcONa; pH 4.5) and DMSO at different ratios. The reaction mixture was stirred at 45 or 60 °C. Then 10−80 equiv of aniline (with respect to the HA) was added to the mixture. Aliquots were taken every 24 h during 7 days and analyzed by GPC. The product from the reactions with the best yields was freeze-dried and ultrafiltered with a cellulose membrane (cut off 30 kDa). Additional details about the influence of the solvent, reaction time, degree of substitution of *N*-hydroxyphthalimide, temperature, HA excess, and catalyst are provided in the Supporting Information.

2.5. Synthesis of Rhodamine (Rho)-Labeled HA Polymers (1−3). HA polymer (15 mg of HMW HA (**1**), 45 mg of LMW HA (**2**), or 10 mg of HA-*g*-HEMA with 8 HA chains, (**3**)) was dissolved in water (0.25 mL). A solution of rhodamine isothiocyanate in DMSO (4 mol % to HA disaccharide, i.e., 0.806 mg in 1 mL for **1** and **2** or 0.19 mg for **3**) was then added to the reaction and stirred for 24 h. The product was purified by ultrafiltration with a cellulose membrane (1 kDa cut off). The solution of the product was concentrated and then ultrafiltrated against 200 mM NaCl (4×) and water (4×) and finally freeze-dried. All procedures were performed under light protection. The Rho-modified HA polymers were characterized by GPC, where no difference in retention time was observed when compared to the unmodified polymers. The degree of modification was assessed by spectrophotometry and fluorescence spectroscopy. For spectrophotometry, standard solutions of rhodamine B were prepared at concentrations between 4 μM and 300 μM in Milli-Q water. Rho-labeled HA polymers were dissolved in Milli-Q water (1 mg/mL), and an absorption spectrum was acquired at wavelengths λ = 450 and 600 nm in a Synergy HT microplate reader (Bio-Tek Instruments, USA). Rhodamine concentration was determined at the maximum absorbance peak (λ_{max} 562 nm). For fluorescence spectroscopy, standard solutions of rhodamine B were prepared between 85 and 200 nM in Milli-Q water, and Rho-labeled HA polymers were diluted to 50 μg/mL in Milli-Q water. Rhodamine B was excited at λ_{ex} 520 nm, and the fluorescence spectrum was acquired between 550 and 650 nm in FP-8500 Spectrofluorometer (Jasco Corp., Japan). The rhodamine B concentration was determined according to the peak area. The degree of modification was determined by the molar ratio between rhodamine B and HA disaccharides (Table S2).

2.6. Nuclear Magnetic Resonance (NMR) Spectroscopy. NMR spectra were recorded on a Bruker AVANCE 400 spectrometer. D_2O, DMSO-d_4, or $CDCl_3$ were used as solvents. Chemical shifts are reported in ppm (δ units) downfield from internal tetramethylsilane when $CDCl_3$ was used as a solvent or 3-(trimethylsilyl)propionic acid-d_4 when the spectra were taken in D_2O.

2.7. Gel Permeation Chromatography (GPC). GPC characterization of the HEMA homopolymer was performed on a LC system consisting of an Agilent-SECcurity-Pump and an Agilent-SECcurity Autosampler connected to a refractive index (PSS-SECcurity DRI) and multiangle static light scattering (PSS SLD 7100 MALLS) detectors. Sample separation was achieved using four columns (PSS, Mainz, Germany): PSS GRAM (Guard, 10 μm, 8 × 50 mm), PSS GRAM (10 μm, 8 × 300 mm, 100 Å), 2× PSS GRAM (10 μm, 8 × 300 mm, 3000 Å). The column and detectors were kept at 70 °C. Samples were eluted with 57 mM LiBr in *N*,*N*-dimethylformamide at a constant rate of 1 mL/min. The light scattering detector was calibrated with a polystyrene narrow standard (PSS, Mainz, Germany) of M_w 87600 kDa and polydispersity index (PDI) 1.08. The d*n*/d*c* was set to 0.065 according to the literature.[37,38] GPC characterization of HA and HA-*g*-HEMA was performed with a Malvern Viscotek TDA 305 with a refractometer (RI-Detector 8110, Bischoff), right and low angle light scattering (RALS and LALS), and viscometer detectors on a set of four columns: precolumn Suprema, 5 μm, 8 × 50 mm, Suprema 30 Å, 5 μm, 8 × 300 mm, and 2× Suprema 1000 Å, 5 μm 8 × 300 mm. The system was kept at 30 °C. We have used phosphate-buffered saline (0.01 M phosphate buffer, 0.0027 M potassium chloride and 0.137 M sodium chloride, pH 7.4, at 25 °C) and 0.05% w/v NaN_3 as an eluent that was pumped at a rate of 1 mL/min. The absolute molecular weight was determined by calibrating the RI, LS (90 and 7°), and viscosity detectors using the software Omnisec 5.12 (ViskoteK) and pullulan (number-average molecular weight, M_n 48.8 kDa and PDI 1.07) as a standard. The d*n*/d*c* of HA (0.15 mL/g) was taken from the literature.[39] For HEMA-*g*-HA copolymers, the d*n*/d*c* was determined online or estimated from the mass percentage of HA and HEMA calculated from NMR. The apparent (i.e., relative) molecular weight was determined after a conventional calibration performed with a commercial polysaccharide set from Polymer Standard Sevive GmbH that contains 10 Pullulans with narrow polydispersity and M_p (molecular mass at the peak maximum) ranging from 180 Da to 708 kDa.

2.8. Dynamic Light Scattering (DLS). The size of the obtained complexes was analyzed on a Malvern NanoZS instrument with a He−Ne laser. DLS and ζ potential measurements were performed at an angle of 173° and room temperature. The average hydrodynamic radius (Rh) and polydispersity index (PDI) were determined by fitting the correlation function with the cumulant method. The polymers were dissolved at concentrations of 1−0.2 g/L in the same buffer used for GPC for comparison purposes.

2.9. Isothermal Titration Calorimetry (ITC). Single-injection ITC kinetics measurements were performed on MicroCal PEAQ-ITC (Malvern, UK). In a single injection ITC experiment, the total heat measured is proportional to the apparent enthalpy (ΔH_{app}) and the number of moles of generated product. The reaction rate is related to the amount of heat generated over time. From the derived Michaelis−Menten plots, the affinity for the substrate (K_M), turnover rate (K_{CAT}), and catalytic efficiency ($K_{EFF} = K_{CAT}/K_M$) values were obtained. We used bovine testicular HYAL (Type I-S, Aldrich H3506, Batch SLBR736 V, 451 units/mg) for these measurements because it catalyzes the hydrolysis of the β(1,4) bonds in HA similarly to human HYAL.[40] All ITC experiments were performed at 37 °C in PBS. A HYAL solution in PBS was placed in the cell of the equipment, and the solution of HA polymer in PBS was loaded in the syringe. All solutions were prepared prior to the experiments and used in the next 1−8 h. Initial experiments were performed at concentrations of HA polymers in the range of 0.5−2 g/L and HYAL solutions of 0.75−3 g/L. The best thermograms were obtained when HA of 1 g/L and HYAL of 1.5 g/L were used. At these concentrations, single injection experiments were performed by injecting 10, 20, and 35 μL with a speed of 0.5 μL/s and a reference power of 20 μcal/s. The thermograms were recorded until an equilibrium was reached (15 min after the last injection). Control experiments were performed to compare the heat generated by the dilution of HA in PBS and the addition of PBS into HYAL to the heat generated by the enzymatic reaction. Apparent enthalpy of the reaction, heat rate (d*Q*/d*t*), and Michaelis−Menten plots were obtained using MicroCal PEAQ-ITC Analysis Software (Malvern). The molar concentrations to calculate K_M are expressed as a concentration of cleavable sites.[41] Such expression of K_M is appropriate for kinetic experiments that follow each cleavage event because in our case cleaved HA polymers generated by HYAL are also HYAL substrates that contain cleavable sites.

2.10. Surface Plasmon Resonance (SPR). The SPR analysis was performed on a Biacore X100 instrument (GE Healthcare, Germany) using PBS containing 0.005% Tween 20 (pH 7.4) at 25 °C as running buffer. The CD44 protein (human recombinant, Fc fusion, biotin-labeled, 50.6 kDa, BPS Bioscience, USA; 25 μg/mL) was immobilized onto a streptavidin-functionalized chip (Cytiva) according to the manufacturer recommendations (15 min, 5 μL/min). A blank chip, i.e., without CD44 immobilization, was used as a reference. Solutions of **1**−**3** were prepared at a range of concentrations (25−200 ng/mL) in the running buffer. Increasing concentrations of each HA polymer were successively injected (30 μL/min) for 180 s (association) followed by a 180 s running buffer (dissociation). The regeneration was achieved with 100 mM glycine·HCl at pH 2.0 for 30 s in the case of **2** or with 1 M NaCl in 50 mM NaOH for 30 s when **1** and **3** were tested. Preliminary results showed that around 50% of CD44 could be regenerated after interaction with **3**, and full recovery was observed

https://doi.org/10.1021/acsami.2c11864
ACS Appl. Mater. Interfaces XXXX, XXX, XXX−XXX

for **1** and **2**. To overcome this technical issue, high CD44 immobilization levels were used to provide enough sensitivity (ng/mL range) and allow total CD44 regeneration.

Kinetic constants (Table S3) were determined by a two-state reaction model in BIAevaluation 2.0.2 software. The two-state binding model assumes 1:1 binding of analyte (HA or HEMA-*g*-HA; *A*) to an immobilized ligand (CD44, *B*) followed by a conformational change that stabilizes the complex (*AB**) and is described by eq 1

$$A + B \underset{k_{a1}}{\overset{k_{d1}}{\rightleftarrows}} AB \underset{k_{a2}}{\overset{k_{d2}}{\rightleftarrows}} AB^* \quad (1)$$

where k_{a1} and k_{d1} are the association and dissociation constants of the binding of the analyte to the ligand and k_{a2} and k_{d2} are the association and dissociation constants of the conformational adjustment of the formed complex.

2.11. Cell Culture and Transfection. Breast cancer cells, MDA-MB-231 and Sk-Br-3, were seeded on tissue culture polystyrene (TCPS) at 37 °C in Dulbecco Modified Eagle Medium (DMEM) high glucose (4.5 g/L) with phenol red (Sigma-Aldrich) supplemented with 3.7 mg/mL sodium bicarbonate (Sigma-Aldrich), 10% fetal bovine serum (FBS, Gibco), and 1% antibiotic/antimycotic (10000 units/mL penicillin G sodium, 10000 μg/mL streptomycin sulfate, and 25 μg/mL amphotericin B in 0.85% saline; Gibco). Breast epithelial cells, MCF10A, were cultured in complete Mammary Epithelial Cell Growth Medium (MEGM, Lonza) at 37 °C. Upon confluence, the cells were detached with TrypLE Express (Gibco) and used in the following experiments at a cell density of 5×10^4 cells/cm^2.

Sk-Br-3 cells were transfected with GFP-tagged CD44 (human, transcript variant 7, NM_001202556, Origene, 25 ng) using Lipofectamine 3000 (Invitrogen) according to manufacture instructions. After 48 h incubation, cells were selected and cultured in the above-described medium supplemented with 1 μg/mL of Geneticin. Cells were used up to passage number 3 after transfection.

2.12. Fröster Resonance Energy Transfer (FRET) Microscopy. CD44-GFP was used as a donor, and Rho-labeled HA polymers were used as acceptors. CD44-GFP-transfected Sk-Br-3 cells were seeded in an 8-well μ-slide polymer coverslip (ibidi), allowed to adhere for 24 h, and then supplemented with Rho-labeled HA polymer dissolved in a culture medium (50 μg/mL) for 30 min at 4, 25, and 37 °C. FRET was observed only at 4 °C due to fast internalization of **1**−**3** at higher temperatures. Cultures with medium alone were used as controls. Cells were fixed with 10% formalin and washed with PBS. Sensitized FRET images were acquired on a confocal laser scanning microscope (TCS SP8, Leica) with a 63× water immersion objective with 512 × 512 px resolution for quantitative proposes and 2048 × 2048 px resolution and 3× virtual magnification for the acquisition of representative images. Fluorescence images were acquired sequentially through sensitized fluorescence emission (λ_{ex} = 488 nm and λ_{em} = [571−700] nm), Rho emission (λ_{ex} = 561 nm and λ_{em} = [571−700] nm), and GFP emission (λ_{ex} = 488 nm and λ_{em} = [498−563] nm. Acquired images were processed by ImageJ 1.53c software. Stacks were projected to a sum. Region of interest was defined at the cell membrane and it was used to measure CD44-GFP and FRET intensity. The ratio between FRET signal and CD44-GFP was used as an indicator of FRET efficiency.[12,16]

2.13. Internalization of 1−3 by MDA-MB-231 and Sk-Br-3. MDA-MB-231 and Sk-Br-3 were cultured for 24 h as described above and then supplemented with Rho-labeled HA polymers (25 μg/mL) for 2 h at 37 °C. The HA polymers were dissolved directly in the culture medium. Cells were then fixed with 10% formalin and stained for actin with phalloidin-FITC (250 ng/mL) and for nuclei with DAPI (1 μg/mL). Fluorescence images were acquired using a confocal laser scanning microscope (TCS SP8, Leica) with a 63× water immersion objective with 512 × 512 px resolution. Images were processed and analyzed in ImageJ 1.53c software. Stack images were sum projected, and cell boundaries (region of interest) were determined according to the phalloidin signal and used for Rho fluorescence measurement. At least 40 cells per condition were analyzed.

2.14. Digestion of Endogenous HA. MDA-MB-231 and Sk-Br-3 cells were seeded on tissue culture polystyrene (TCPS) coverslips for 24 h and then supplemented with HYAL (type IV-S from bovine testes, 750−3000 units/mg) at a concentration of 250 μg/mL (2 μL; 1 h).

2.15. Evaluation of Cell Viability. MDA-MB-231, Sk-Br-3, and MCF10A cells were cultured and supplemented with **1**−**3** at different concentrations (0, 25, 50, or 100 μg/mL) for 2 and 24 h. MTS was performed according to the manufacturer's instructions. Briefly, after incubation, the cell culture medium was replaced by MTS medium (DMEM low glucose without phenol red supplemented with 10% FBS, 1% antibiotic/antimycotic and 1:5 volume ratio of CellTiter 96 AQueous One Solution Cell Proliferation Assay) and incubated for 3 h at 37 °C. Then, 100 μL of MTS medium was transferred to a transparent 96-well plate, and absorbance was measured at 490 nm in a microplate reader (Synergy HT, Biotek).

2.16. Evaluation of CD44 Clustering. MDA-MB-231 cells were cultured and supplemented with **1**−**3** (100 μg/mL, 2 h) as described above. Cells were washed with PBS, detached from the TCPS with 4 mM EDTA in PBS (pH 8), and washed again with PBS. CD44 clusters were cross-linked by incubation with 2 mM bis-(sulfosuccinimidyl) suberate (BS^3) (Sigma) for 1 h at 4 °C followed by incubation with 20 mM Tris (pH 7.5) for 15 min at rt for quenching. Cells were washed with PBS twice and lysed with RIPA lysis buffer. The protein lysate was incubated over ice for 30 min with cycles on the vortex and centrifuged (13000*g*, 20 min, 4 °C). Protein concentration in the supernatant was determined by BCA protein assay according to the manufacturer's instructions (ThermoFisher Scientific). Equal protein amounts were separated in Bolt 8% Bis-Tris gel (Thermofisher Scientific) with Bolt MES SDS Running Buffer (Thermofisher Scientific) and transferred onto a PVDF membrane. The membranes were blocked with 5% BSA in Tris-buffered saline containing 0.1% Tween-20 (TBS-T) for 30 min at room temperature and incubated with monoclonal antibody to CD44 [8E2F3] (diluted 1:5000, OriGene) and with anti-GAPDH antibody [EPR16891] (diluted 1:10000, abcam) at 4 °C overnight. Then membranes were washed with TBS-T and incubated with antirabbit and antimouse IRDye (diluted 1:10000, Li-Cor) in 1% BSA/TBS-T for 1 h at rt. After washing with TBS-T and TBS, blots were visualized using Odyssey Fc Imaging System (Li-Cor). Densitometry analysis was carried by ImageJ 1.53c software. CD44 signal was normalized to the lane using the GAPDH as a loading control.

2.17. Statistical Analysis. All experiments were repeated at least in duplicate in two independent experiments. The results are presented as mean ± standard deviation. The data failed to show homogeneity of variances; therefore, the Kruskal−Wallis test was used to test differences between groups with 95% significance for multicomparison between conditions. the Benjamini and Hochberg p-adjusting method was used.

3. RESULTS AND DISCUSSION

3.1. Synthesis of HA Brush Copolymers. There are different molecular designs of HA copolymers: most of them are based on the grafting of synthetic polymer chains at the −COOH groups of HA, and only a few examples are reported in which HA is end-on linked (i.e., at the reducing end) to a synthetic core. These examples include diblock copolymers[42−45] and glycopolymers made of a synthetic core with short (mono-, di-, and tetrasaccharides) glycan branches.[46−48] The synthetic core can vary to control the molecular architecture of the glycopolymer, while the glycan branches determine the selectivity, specificity, and avidity in the biointeractions of these polymers. Previously, we have reported the preparation of star-like copolymers with long HA branches and a hyperbranched polyglycerol core (HPG).[49] The molecular weight (M_w) of this core is relatively low as HPG

https://doi.org/10.1021/acsami.2c11864
ACS Appl. Mater. Interfaces XXXX, XXX, XXX−XXX

with high M_w, and low polydispersity indexes (PDI) are challenging for synthesis.[50] The copolymers presented herein also contain long HA branches with preserved structure/bioactivity, but the synthetic core is linear. The use of this molecular design has several advantages. It allows introduction of a higher number of HA chains by increasing the M_w of the core (in hyperbranched structures, the conjugation sites can be buried/sterically hindered). Additionally, a linear core is adequate to obtain an extended structure with enough spacing between the HA chains to enable multivalent interactions of these branches. We used a polyhydroxyethyl methacrylate (HEMA) core, which can be synthesized by atom transfer radical polymerization (ATRP, Figure 1D) that permits to obtain polymers with on-demand M_w and low PDI.[36] Moreover, HEMA is widely used in the biomedical field, and one of the reasons is the free −OH groups that can be functionalized to generate copolymers.[51,52] Herein, we synthesized and used HEMA with the following characteristics: M_n 62.4 kDa, M_w 74.6 kDa, PDI 1.20 (SI, Figures S1 and S2).

To graft HA via its reducing end, we first obtained HEMA-*N*-hydroxyphthalimide by the Mitsunobu reaction followed by hydrazine deprotection to generate aminooxy groups needed for an oxime ligation (Figure 1D). Previously, we have used oxime coupling to prepare diblock and star-like copolymers of GAGs and have demonstrated that this coupling preserves the bioactivity of the grafted GAG.[49,53] Of note, we initially used an excess of phthalimide for the Mitsunobu reaction aiming to generate maximum possible reactive sites. However, the copolymers obtained at these conditions had low solubility in the solvent system/conditions usually used for the next oxime coupling. We, therefore, performed an extensive optimization of the coupling conditions (temperature, solvent, catalysts, and polymers with varying degrees of aminooxy functionalization, SI, Tables S1 and S5, Figures S3−8). The highest conversion rate (∼44% of HA into HA-*g*-HEMA) was obtained when we used HEMA-ONH_2 polymers with 25% of −OH groups substituted by −ONH_2 groups in DMSO/acetate buffer at 60 °C. At these conditions, we generated HA-*g*-HEMA copolymers with a different number of HA chains by tuning the HA stoichiometry (SI, Table S5, Figures S6−8).

The obtained copolymers were characterized by nuclear magnetic resonance (NMR, SI, Figures S6−8) and gel permeation chromatography (GPC, SI, Figures S4−5) with viscosity and light-scattering detectors. NMR showed the presence of oxime at the distinctive chemical shifts, i.e., between 6.5 and 8 ppm,[49,53] and was used to determine the degree of substitution (DS) of HEMA-ONH_2 and the number of HA chains linked to the HEMA core. A very high absolute molecular weight (abs M_n) and short retention times, i.e., high apparent molecular weight (app M_n), were obtained for HA-*g*-HEMA with low DS (as determined by NMR) (SI, Table S5).

This behavior can be explained by the above-mentioned low solubility of HEMA-ONH_2 in water. The polymers with low DS aggregate (see SLS and DLS below) in water and aqueous media, e.g., buffer solutions. On the other hand, the polymers with high DS have longer retention times associated with a lower app and abs M_n because they are dissolved and do not aggregate, and the determined abs M_n is similar to the M_n estimated by NMR (SI, Table S5). To confirm that the polymers with longer retention times have indeed higher DS, the oxime linkage was hydrolyzed in acid media and the released HA was quantified by GPC (SI, Table S5).

The GPC analysis with light scattering (at two angles) and viscosity detectors also allowed to determine the radius of gyration (Rg) and the hydrodynamic radius (Rh) of the polymers in solution (SI, Table S5; data for HA are included for comparison in Table S4). HA-*g*-HEMA with low DS had Rg/Rh (Rg 35 nm, Rh 31 nm, Rg/Rh = 1.1) that is typical for spherical structures (e.g., polymer micelles)[54] confirming the proposed aggregation. For the copolymers with intermediate DS, we obtained Rg/Rh ratio similar to HA (Rg 30 nm, Rh 16 nm, Rg/Rh = 1.9), which corresponds to a semirigid structure.[55] The Rg/Rh determined for the HA-*g*-HEMA with the highest DS (Rg 26 nm, Rh 11 nm, Rg/Rh = 2.3) agrees with a rigid structure found in densely modified copolymers with soluble grafts.[55] The aggregation of the copolymers was investigated by dynamic light scattering (DLS, Table S5). The DLS data followed the same trend as the observed by static light scattering (SLS detector used in GPC analysis) but the obtained Rh were higher (196, 72, and 38 nm for the polymers with low, medium, and high DS, respectively). The difference between DLS and SLS is bigger for the polymer with lowest DS and agrees with the overestimated M_n by GPC confirming the above-mentioned aggregation (large aggregates are broken in the GPC). The aggregation of the low DS polymer and better solubility of the polymer with higher DS was also supported by the obtained polydispersity indexes (PDI) of DLS that were 0.37 for low DS, which is at the limit between micellar and a polymer solution, and above 0.5 for higher DS corresponding to polymers in solution (Table S5). Altogether, these data showed that the Rg/Rh derived from GPC is indicative for a spherical polymer conformation rather than for the presence of homogeneous micelles. For the following experiments, we selected HA-*g*-HEMA with intermediated DS (**3**), i.e., DS of 1.6, which corresponds to 8 grafted HA chains.

3.2. Degradation of HA Polymers by Hyaluronidase (HYAL). Because the fragmentation of HA is crucial for its biological activity, we studied the degradation of **1**−**3** by HYAL. The HYAL mechanism of action is complex: it acts in an endolithic random fashion and catalyzes the break of $\beta(1,4)$ bonds in HA and chondroitin sulfates, but at final degradation stages it also promotes the recombination of the generated dimers to form tetramers.[40,56,57] HYAL is a nonprocessive enzyme (i.e., it releases the substrate before the next hydrolysis) that forms a complex with a tetrasaccharide, and there are no reports about the simultaneous binding of several HYAL molecules to a long HA chain.[40] In spite of its complex mechanism of action, HYAL kinetics follows the Michaelis−Menten law as shown by UV spectrometry,[56,58] GPC,[59] or electrophoresis combined with UV or mass spectrometry.[60] Herein, we used single-injection experiments to determine the kinetics parameters for the degradation of **1**−**3** by HYAL. Isothermal titration calorimetry (ITC) is a relatively new method for studying enzyme kinetics; in 2001, it was demonstrated for the first time that *in situ* determination of the reaction heat can be used for precise and fast acquisition of the Michaelis−Menten parameters.[61,62] ITC is time- and sample-saving as the experiment consists of a simple mixing of minimal amount (microliters) of enzyme and substrate. Moreover, the obtained data are straightforward; i.e. there is no need to determine the formation of new species (reducing sugars or oligosaccharides) as it is done in common methods and therefore, any uncertainty derived from the selected technique (UV, mass spectrometry, GPC) and systematic

https://doi.org/10.1021/acsami.2c11864
ACS Appl. Mater. Interfaces XXXX, XXX, XXX−XXX

errors are abolished. We could not find previous reports on the use of ITC for studying the HYAL action on HA. The concentrations of the substrates and the enzyme were optimized to obtain a full conversion within minutes and enough heat to avoid the dilution effects in the thermograms (see the SI for details). This information was then expressed in terms of reaction rate and fitted to the Michaelis–Menten equation to obtain the main kinetic parameters (Table 1, Figures S9 and S10).

Table 1. Affinity for the Substrate (K_M, Michaelis Constant), Turnover Rate (K_{CAT}), and Catalytic Efficiency (K_{EFF}) of the Degradation of Substrates 1–3 by HYAL Determined by Isothermal Titration Calorimetry (ITC, n = 3) and Michaelis–Menten Equation

substrate	K_M (μM)	K_{CAT} (s^{-1})	K_{EFF} (μM^{-1} s^{-1})
HMW HA (**1**)	607 ± 150	(69 ± 10) × 10^{-2}	1150 ± 108
LMW HA (**2**)	772 ± 250	(80 ± 14) × 10^{-2}	1007 ± 169
HEMA-*g*-HA (**3**)	284 ± 75	(22 ± 6) × 10^{-2}	766 ± 18

The obtained K_M agrees well with the data obtained by other methods and reported in the literature.[41,56,58,63] The K_M determined for **3** is smaller (higher affinity) as compared to **1** and **2** (Table 1). This difference can be explained by a higher stoichiometry, i.e., binding of more than one HYAL to the brush-like structure of **3**. The semirigid structure of **3** with different exposed and extended HA branches makes the multiple binding in the brush structures more probable than in native HA.[64] In fact, similar multiple binding of HYAL has been reported recently for nanoparticles with surface-exposed HA (also of ca. 5 kDa).[45] These nanoparticles inhibit the degradation of HMW HA by HYAL via competitive binding of the enzyme.[45]

The ITC also allows to determine the hydrolysis rate (K_{CAT}). Besides the high affinity of HYAL to **3**, we observed lower K_{CAT} (slow hydrolysis) for the copolymer when compared to **1** and **2**. Such a slower reaction rate can be due to an inefficient enzyme release from the more crowded complex **3**/HYAL (i.e., nonprocessive enzyme). The smaller K_{CAT} and K_M results in significantly lower K_{EFF}, showing that the hydrolysis takes longer for **3**, which might have important biological consequences.

3.3. Interaction of HA Polymers with CD44. To further check the effect of the multivalent HA presentation, we have investigated the interactions of **1**–**3** with CD44, the main HA receptor, by several characterization methods. A real-time interaction was followed by surface plasmon resonance (SPR, Figure 2).

The obtained sensograms for **1** and **2** (Figure 2A, B) agree with previously reported data for HA: **1** binds steady and remains attached to CD44 because of the multivalent interactions with the long HA chains, while **2** binds and detaches rapidly from the functionalized sensor surface.[44,65] The sensogram of **3** (Figure 2C) is different from **1** and **2**: at first sight, it shows binding kinetics similar to the observed for **2** and a dissociation similar to **1**, while there is some loosely bound **3** that is released at the beginning of the dissociation process, most of the polymer remains attached to the surface. To render quantitative information (Table 2), the sensograms were fitted (Figure 2, black line) with a two-state reaction model. This model was chosen because of the reported CD44 conformational change upon HA binging.[66] It assumes a 1:1

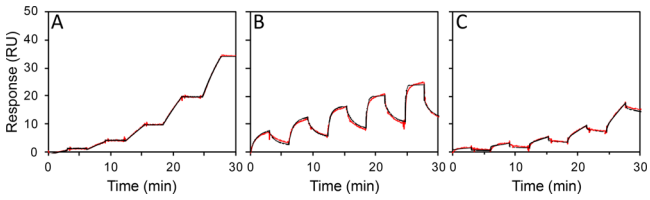

Figure 2. Representative SPR sensograms showing the kinetics of the CD44 interactions with (A) HMW HA (1), (B) LMW HA (2), and (C) HA-*g*-HEMA (3). Solutions with increasing concentrations of HA polymer (12.5–200 ng/mL) were injected stepwise over the chip with immobilized CD44. Each of these injections was followed by a dissociation step. The raw data are presented in red and the fitting in black. The respective constants are shown in Table 2.

binding between ligand and protein with a subsequent conformational change of the ligand[67] and in the case of **1** and **3**, the affinity reflects the average association. The alternative heterogeneity model presumes 2–4 binding sites,[65] which does not reflect the real stoichiometry (the binding domain of CD44 is a HA octasaccharide;[68] i.e., **1** has ca. 800 possible binding sites). We also applied this model to the obtained SPR data but the fitting was not as good as the one obtained with the two-state model. The binding kinetics depends on the surface density of active CD44 too.[69] Considering the M_w of CD44 and the Rg of **1**–**3**, we estimated the surface density of CD44 (details in the SI) and the respective number of CD44 molecules available at the surface per ligand (SI, Table S4): **1** can interact with 477 CD44 molecules; **2** has only with 0.3 CD44, and therefore can bind only one CD44 under the tested SPR experimental conditions; and **3** can interact with 25 CD44 molecules to bind via HA octasaccharides.

Despite the model differences, the K_A values obtained for **1** and **2** ($K_A(\mathbf{1}) > K_A(\mathbf{2})$) are in good agreement with previously reported data obtained from SPR kinetic assay and from the binding of fluorescein-conjugated HA to CD44 expressing cells.[70,71] The analysis of the K_1 and K_2 indicates adequate selection of the model: $K_1(\mathbf{1}) \gg K_1(\mathbf{2})$ due to the binding of several CD44 to **1** and 1:1 binding stoichiometry for **2**:CD44. $K_2(\mathbf{1}) \gg K_2(\mathbf{2})$ shows greater conformational freedom/changes upon binding of CD44 to **1**. An intermediate K_A was determined for **3**. An increased avidity is observed for this copolymer: **3** has 8 HA branches with the size of **2** but has more than 2500-fold higher K_A than **2**. The $K_2(\mathbf{3})$ is similar to $K_2(\mathbf{1})$, showing that besides the avidity, the interactions between **3** and CD44 benefit from conformational adjustments similar to the ones determined for **1**. These results indicate a zipper-like mechanism of interactions between the copolymer and CD44: once one of the branches interacts with CD44, the other LMW HA chains are brought closer to CD44 and their recognition/association with this receptor is promoted. In the brush structure of **3**, the 8 LMW HA chains are relatively separated (the degree of polymerization of HEMA is 480; i.e., there is one HA branch for every 60 HEMA monomers), which allows conformational freedom as indicated by $K_2(\mathbf{3})$ and is beneficial for the proposed mechanism.

3.4. Effect of HA Polymers on CD44 Expression and Clustering In Vitro. We selected two breast cancer cell lines, MDA-MB-231 and Sk-Br-3, to demonstrate the effect of **3** in vitro. These cells differ by the expression of CD44 and HA:[12,72–74] MDA-MB-231 cells have high CD44 expression (CD44+) and a considerable amount of endogenous HA at the

https://doi.org/10.1021/acsami.2c11864
ACS Appl. Mater. Interfaces XXXX, XXX, XXX–XXX

Table 2. Quantitative Data for the Interactions between CD44 and 1−3 Obtained from the Surface Plasmon Resonance Sensograms Fitted to a Two-State Reaction Model (n = 3): Equilibrium Constants of the Two States (K_1 and K_2), Association Constant of the Binding (K_A)

ligand	K_1 [M^{-1}][a]	K_2 [M^{-1}]	K_A [M^{-1}]
HMW HA (**1**)	$(4.1 \pm 3.8) \times 10^{11}$	$(1.1 \pm 1.8) \times 10^{3}$	$(3.3 \pm 5.7) \times 10^{13}$
LMW HA (**2**)	$(2.9 \pm 1.8) \times 10^{6}$	4.1 ± 0.3	$(1.5 \pm 0.9) \times 10^{7}$
HEMA-*g*-HA (**3**)	$(7.8 \pm 10) \times 10^{7}$	$(3.0 \pm 5.2) \times 10^{3}$	$(4.0 \pm 6.0) \times 10^{10}$

[a]Sensograms (triplicate) were fitted to obtain the kinetic constants, ka_1, kd_1, ka_2, and kd_2 for the two-state reaction model. Then $K_1 = ka_1/kd_1$ and $K_2 = ka_2/kd_2$ were calculated; the association constant was calculated from the equation $K_A = K_1(1 + K_2)$. All fitted parameters and equations are included in the SI.

pericellular space (SI, Figure S12A). In contrast, Sk-Br-3 cells have a low expression of HA and CD44 (CD44−), and HA is mainly located in the cytoplasm (SI, Figures S13A and S13B).

Forster resonance energy transfer (FRET) experiments were performed to assess the recognition and binding of the HA polymers **1**−**3** by CD44 in vitro (Figure 3). For these experiments, we used Sk-Br-3 cells (low expression of CD44) that were transfected with green fluorescence protein-CD44 (CD44-GFP).

CD44-GFP has an intense signal at 488 nm (Figure 3A, CTRL CD44-GFP) and very low intensity at 561 nm (Figure 3A, CTRL FRET), i.e., small contribution (6%) from signal bleed-through to the FRET, while Rho has a negligible contribution to FRET (SI, Figure S14). We optimized the polymers binding to the receptors by incubating CD44-GFP expressing Sk-Br-3 cells with **1**−**3** at different temperatures (37 °C, room temperature and 4 °C), and FRET signaling was only observed for cells incubated at 4 °C. Confocal microscopy analysis of the transfected cells showed expression of CD44-GFP mainly at the cell surface (Figure 3A, CD44-GFP: CTRL). Cultures of these cells were then supplemented with Rho-labeled HA polymers (see the SI for details on the characterization of the labeled polymers). FRET data confirmed that indeed the exogenous HA polymers **1**−**3** bind the CD44 (Figure 3A, CD44-GFP: CTRL vs **1**−**3**): we observed a significant increase of the FRET intensity (Figure 3B, red) and FRET/CD44-GFP ratio (Figure 3B, black bars) for cultures supplemented with **1**−**3** as compared to the control.

The effect of **1**−**3** on cell viability was quantified by MTS assay (SI, Figure S15). The results showed no effect on normal human mammary epithelial cells MCF10A and MDA-MB-231 cells viability, but the viability of Sk-Br-3 cells was compromised in a concentration-dependent manner shortly (2 h) after the supplementation with **1**−**3**. However, a recovery occurred 24 h after the supplementation with one exception: only 50% of viability was observed for Sk-Br-3 cultures supplemented with **3** at a concentration of 100 μg/mL. This result indicated that the mechanism of action and bioactivity of **3** might be different from **1** and **2**.

We used Rho-labeled HA polymers to follow the uptake of **1**−**3**. The results showed clearly that **1** and **3** are internalized by the cells, whereas no internalization was visible upon supplementation of **2** (Figure 4). Such different uptake is most probably due to the multiple binding sites in **1** and **3**, making possible the interactions of one molecule with several CD44 receptors, which favors endosome formation and further internalization.[1,16] This process was evident for both cell lines, although a lower internalization was observed for MDA-MB-231 cells (Figure 4B).

At first glance, these results seem contradictory, keeping in mind the high expression of CD44 in MDA-MB-231 cells. However, these cells are also coated with a dense matrix of endogenous HA that competes with the exogenous HA for CD44 binding, thus interfering with the internalization process.[16] On the other hand, Sk-Br-3 cells lack such a pericellular HA coat; i.e. the surface receptors are more exposed to the supplemented HA polymers.[10,12]

To check if indeed **3** competes with endogenous HA for CD44 binding in MDA-MB-231 cells and, thus, might affect CD44 clustering, we performed a chemical cross-link of the protein at the cell surface and quantified the cross-linked CD44 (Figure 5).

Western blot analysis showed an additional band for the control samples after the applied cross-linking (Figure 5A, the band nCD44); i.e. the CD44 receptors in these cells are clustered. Supplementation with **1** did not significantly influence CD44 clustering, while **2** and **3** significantly decreased the CD44 clustering ($p < 0.0001$). Moreover, more efficient CD44 declustering was observed in the presence of **3** when compared to **2**, which agrees with the higher binding affinity of **3** to CD44 as determined by SPR experiments.

The same procedure was applied to MDA-MB-231 cells after digestion of the endogenous HA (Figure 5B). For these cells, all exogenous HA polymers disrupted the CD44 clustering but at different magnitude. The lowest declustering effect was observed in the presence of **1**. As discussed above, cells can degrade the supplemented HMW HA; i.e., it provides a source of HA fragments that have attenuated the effect of LMW HA. The most pronounced effect on the CD44 clustering was observed for **3** followed by **2**.

The disruption of CD44 clusters by LMW HA has already been studied in HK-2 and BT-549 cell lines, which have very high expression of CD44 and agree with our results: this previous study reports that LMW HA induced disruption of CD44 clustering in a concentration-dependent fashion and competes with endogenous HA for the same binding site on CD44.[16] A comparison of the data obtained for MDA-MB-231 cells with and without HYAL treatment supports that indeed the declustering activity of **2** and **3** results from the competition for CD44 binding with the endogenous HMW HA in the pericellular space and therefore is not observed for **1**. Altogether, our results demonstrated that HA-*g*-HEMA is an efficient platform to target CD44 clustering with a higher affinity than LMW HA.

4. CONCLUSIONS

We showed that oxime condensation is a feasible and versatile synthetic route to prepare hybrid glycosaminoglycan graft copolymers with different densities of the glycan chains. The grafted chains are in an extended conformation and, thus,

https://doi.org/10.1021/acsami.2c11864
ACS Appl. Mater. Interfaces XXXX, XXX, XXX−XXX

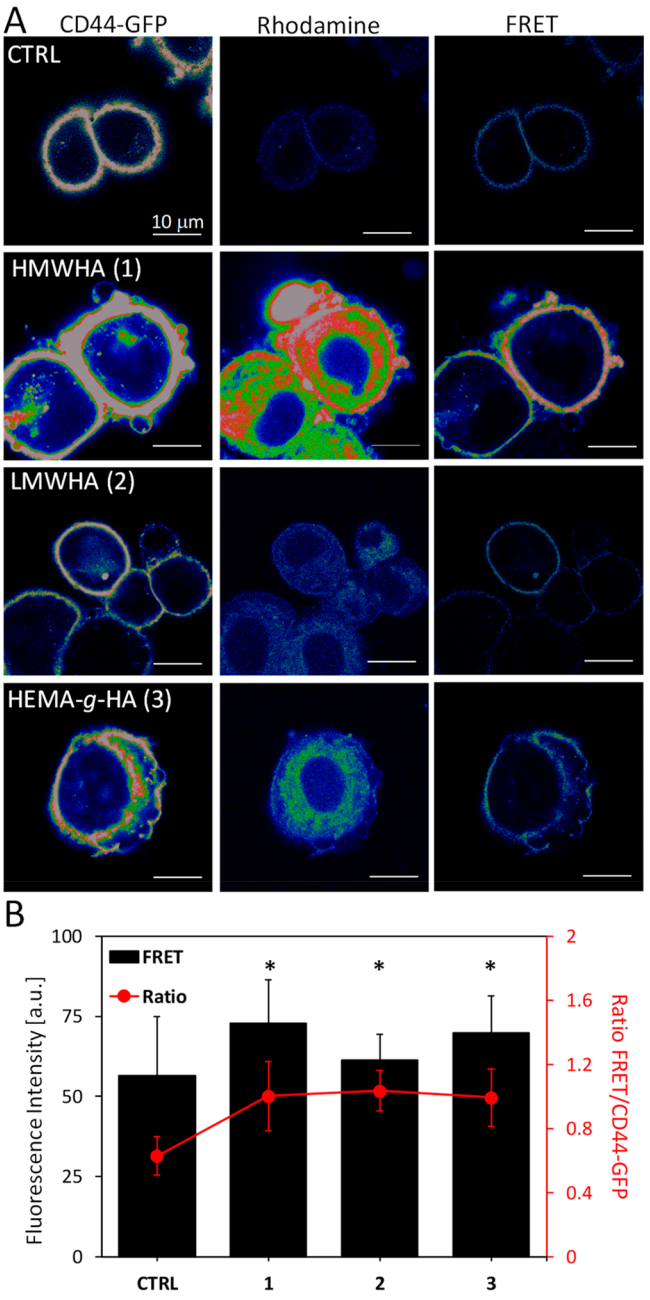

Figure 3. Effect of hyaluronan polymers **1**-**3** on the expression of and binding to CD44 in Sk-Br-3 cells transfected with CD44-GFP. (A) Representative confocal images of Sk-Br-3 cells transfected with CD44-GFP (control, CTRL), cultures supplemented with rhodamine-labeled **1**−**3**, and Forster resonance transfer energy (FRET) for these cultures. (B) Ratio between fluorescence acquired for CD44-GFP and FRET, which indicates the energy transference efficiency of CD44-GFP to Rho. Statistically different from the control at $*p < 0.001$, $n = 3$. Controls are presented in the SI, Figure S14.

optimally exposed to interact with cell surface CD44 in a multivalent fashion, ensuring specificity and high affinity of this interaction. Given its peculiar structure, HA-*g*-HEMA shares some properties with LMW HA (e.g., competitive binding to CD44), while others with HMW HA (internalization by cells, effect on CD44 expression). The most promising bioactivity of the copolymer is the boost of CD44 declustering: its effect is stronger than the one caused by LMW HA. HA-*g*-HEMA also has the advantage of a higher affinity to CD44 and a slower

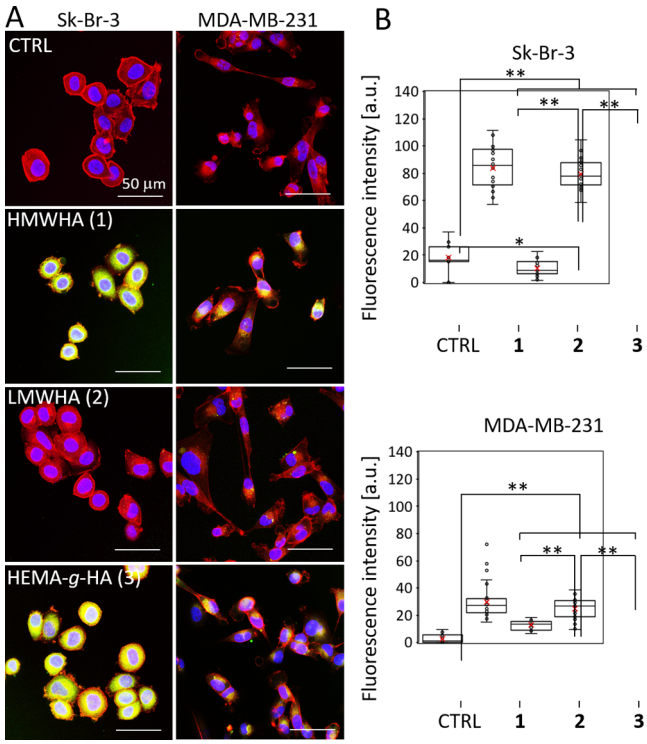

Figure 4. Internalization of **1**−**3** by MDA-MB-231 and Sk-Br-3 cells. (A) Representative confocal images of MDA-MB-231 and Sk-Br-3 cells incubated with rhodamine-labeled polymers (green) and stained for actin (phalloidin, red) and nuclei (DAPI, blue). (B) Quantification of the rhodamine fluorescence intensity for the studied conditions. Statistically significant data are marked with $*p < 0.05$ and $**p < 0.0001$, $n = 3$.

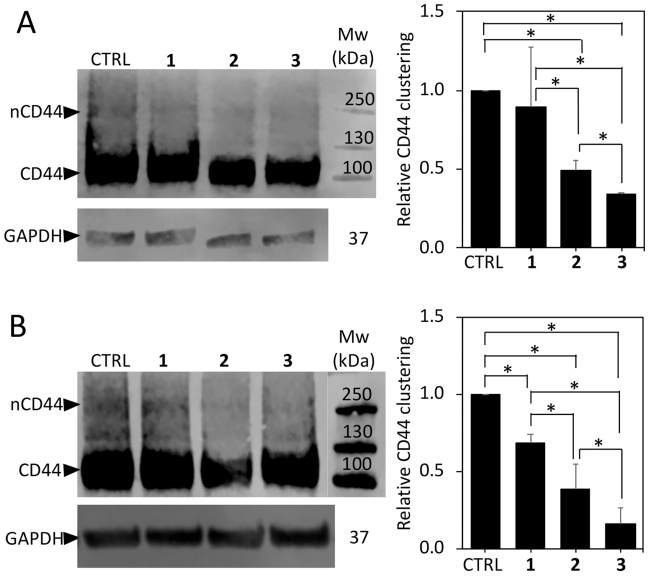

Figure 5. Western blot analysis and the respective densitometry quantification showing CD44 clustering in (A) MDA-MB-231 cells and (B) HYAL-treated MDA-MB-231 cells (cells were treated with 250 μg/mL of HYAL for 1 h) supplemented with **1**−**3** (100 μg/mL, 2 h). The densitometry quantification was normalized to loading control GAPDH and control sample (cells without supplemented HA polymers). Statistical differences are marked with * for $p < 0.05$, $n = 3$.

HYAL degradation, and thus, we foresee its application for tumor targeting and metastasis reduction.

https://doi.org/10.1021/acsami.2c11864
ACS Appl. Mater. Interfaces XXXX, XXX, XXX−XXX

■ ASSOCIATED CONTENT

Supporting Information

The Supporting Information is available free of charge at https://pubs.acs.org/doi/10.1021/acsami.2c11864.

Optimization of the synthesis of HEMA-*g*-HA; characterization data for all polymers (GPC chromatograms, NMR spectra), cells, and controls (PDF)

■ AUTHOR INFORMATION

Corresponding Authors

Ramon Novoa-Carballal − *3B's Research Group, I3Bs − Research Institute on Biomaterials, Biodegradables and Biomimetics, University of Minho, Headquarters of the European Institute of Excellence on Tissue Engineering and Regenerative Medicine, 4805-017 Barco, Portugal; ICVS/3B's − PT Government Associate Laboratory, 4710-057 Braga/Guimarães, Portugal;* orcid.org/0000-0003-0422-8048; Email: ramon.novoa@i3bs.uminho.pt

Iva Pashkuleva − *3B's Research Group, I3Bs − Research Institute on Biomaterials, Biodegradables and Biomimetics, University of Minho, Headquarters of the European Institute of Excellence on Tissue Engineering and Regenerative Medicine, 4805-017 Barco, Portugal; ICVS/3B's − PT Government Associate Laboratory, 4710-057 Braga/Guimarães, Portugal;* orcid.org/0000-0001-6818-3374; Email: pashkuleva@i3bs.uminho.pt

Authors

Ana M. Carvalho − *3B's Research Group, I3Bs − Research Institute on Biomaterials, Biodegradables and Biomimetics, University of Minho, Headquarters of the European Institute of Excellence on Tissue Engineering and Regenerative Medicine, 4805-017 Barco, Portugal; ICVS/3B's − PT Government Associate Laboratory, 4710-057 Braga/Guimarães, Portugal;* orcid.org/0000-0003-3085-7796

Jesus Valcarcel − *Grupo de Reciclado y Valorización de Materiales Residuales (REVAL), Instituto de Investigacións Mariñas (IIM-CSIC), Vigo 36208 Galicia, Spain;* orcid.org/0000-0001-7336-4049

Diana Soares da Costa − *3B's Research Group, I3Bs − Research Institute on Biomaterials, Biodegradables and Biomimetics, University of Minho, Headquarters of the European Institute of Excellence on Tissue Engineering and Regenerative Medicine, 4805-017 Barco, Portugal; ICVS/3B's − PT Government Associate Laboratory, 4710-057 Braga/Guimarães, Portugal*

Marisa Gomes − *3B's Research Group, I3Bs − Research Institute on Biomaterials, Biodegradables and Biomimetics, University of Minho, Headquarters of the European Institute of Excellence on Tissue Engineering and Regenerative Medicine, 4805-017 Barco, Portugal; ICVS/3B's − PT Government Associate Laboratory, 4710-057 Braga/Guimarães, Portugal*

José Antonio Vázquez − *Grupo de Reciclado y Valorización de Materiales Residuales (REVAL), Instituto de Investigacións Mariñas (IIM-CSIC), Vigo 36208 Galicia, Spain;* orcid.org/0000-0002-1122-4726

Rui L. Reis − *3B's Research Group, I3Bs − Research Institute on Biomaterials, Biodegradables and Biomimetics, University of Minho, Headquarters of the European Institute of Excellence on Tissue Engineering and Regenerative Medicine, 4805-017 Barco, Portugal; ICVS/3B's − PT Government Associate Laboratory, 4710-057 Braga/Guimarães, Portugal*

Complete contact information is available at: https://pubs.acs.org/10.1021/acsami.2c11864

Author Contributions

R.N.-C., J.V., M.G.: polymer synthesis and characterization; R.N.-C.: ITC experiments; A.M.C.: SPR and cell experiments; D.S.C.: cell experiments; R.N.-C. and I.P.: concept and planning; R.N.-C., A.C., and I.P.: writing the manuscript; R.L.R., I.P., R.N.-C., J.A.V.: supervision and funding; all authors read, corrected, and approved the manuscript.

Notes

The authors declare no competing financial interest.

■ ACKNOWLEDGMENTS

The authors thank the Portuguese Foundation for Science and Technology (FCT) for funding (Grants. SFRH/BD/114847/2016, PTDC/QUI-POL/28117/2017, and CEECIND/00814/2017). R.N.C. thanks K. Loos, A. J. Woortman, and Stephan Cairns (MALVERN) for a fruitful discussion on GPC data and R. Pacheco for discussion on ITC data.

■ REFERENCES

(1) Toole, B. P. Hyaluronan: From Extracellular Glue to Pericellular Cue. *Nature Reviews Cancer* **2004**, *4* (7), 528−539.

(2) Liu, M. H.; Tolg, C.; Turley, E. Dissecting the Dual Nature of Hyaluronan in the Tumor Microenvironment. *Frontiers in Immunology* **2019**, *10*, 13856.

(3) Garantziotis, S.; Savani, R. C. Hyaluronan biology: A Complex Balancing Act of Structure, Function, Location and Context. *Matrix Biology* **2019**, *78*−*79*, 1−10.

(4) Amorim, S.; da Costa, D. S.; Freitas, D.; Reis, C. A.; Reis, R. L.; Pashkuleva, I.; Pires, R. A. Molecular Weight of Surface Immobilized Hyaluronic Acid Influences CD44-Mediated Binding of Gastric Cancer Cells. *Sci. Rep.* **2018**, *8*, 16058.

(5) Auvinen, P.; Tammi, R.; Parkkinen, J.; Tammi, M.; Agren, U.; Johansson, R.; Hirvikoski, P.; Eskelinen, M.; Kosma, V. M. Hyaluronan in Peritumoral Stroma and Malignant Cells Associates with Breast Cancer Spreading and Predicts Survival. *Am. J. Pathol.* **2000**, *156* (2), 529−536.

(6) Heldin, P.; Basu, K.; Olofsson, B.; Porsch, H.; Kozlova, I.; Kahata, K. Deregulation of Hyaluronan Synthesis, Degradation and Binding Promotes Breast Cancer. *Journal of Biochemistry* **2013**, *154* (5), 395−408.

(7) Cox, T. R. The Matrix in Cancer. *Nature Reviews Cancer* **2021**, *21* (4), 217−238.

(8) Vignal, P.; Meslet, M. R.; Romeo, J. M.; Feuilhade, F. Sonographic Morphology Of Infiltrating Breast Carcinoma - Relationship with the Shape of the Hyaluronan Extracellular Matrix. *Journal of Ultrasound in Medicine* **2002**, *21* (5), 531−538.

(9) Simpson, M. A.; Wilson, C. M.; Furcht, L. T.; Spicer, A. P.; Oegema, T. R.; McCarthy, J. B. Manipulation of Hyaluronan Synthase Expression in Prostate Adenocarcinoma Cells Alters Pericellular Matrix Retention and Adhesion to Bone Marrow Endothelial Cells. *J. Biol. Chem.* **2002**, *277* (12), 10050−10057.

(10) Veiseh, M.; Kwon, D. H.; Borowsky, A. D.; Tolg, C.; Leong, H. S.; Lewis, J. D.; Turley, E. A.; Bissell, M. J. Cellular Heterogeneity Profiling by Hyaluronan Probes Reveals an Invasive but Slow-Growing Breast Tumor Subset. *Proc. Natl. Acad. Sci. U.S.A.* **2014**, *111* (17), E1731−E1739.

(11) Cieply, B.; Koontz, C.; Frisch, S. M. CD44S-hyaluronan Interactions Protect Cells Resulting from EMT Against Anoikis. *Matrix Biology* **2015**, *48*, 55−65.

(12) Carvalho, A. M.; da Costa, D. S.; Paulo, P. M. R.; Reis, R. L.; Pashkuleva, I. Co-localization and Crosstalk Between CD44 and

RHAMM Depend on Hyaluronan Presentation. *Acta Biomaterialia* **2021**, *119*, 114−124.
(13) Misra, S.; Ghatak, S.; Toole, B. P. Regulation of MDR1 Expression and Drug Resistance by a Positive Feedback Loop Involving Hyaluronan, Phosphoinositide 3-kinase, and ErbB2. *J. Biol. Chem.* **2005**, *280* (21), 20310−20315.
(14) Lee, J. T.; Steelman, L. S.; McCubrey, J. A. Phosphatidylinositol 3 ′-kinase Activation Leads to Multidrug Resistance Protein-1 Expression and Subsequent Chemoresistance in Advanced Prostate Cancer Cells. *Cancer Res.* **2004**, *64* (22), 8397−8404.
(15) Slomiany, M. G.; Grass, G. D.; Robertson, A. D.; Yang, X. Y.; Maria, B. L.; Beeson, C.; Toole, B. P. Hyaluronan, CD44, and Emmprin Regulate Lactate Efflux and Membrane Localization of Monocarboxylate Transporters in Human Breast Carcinoma Cells. *Cancer Res.* **2009**, *69* (4), 1293−1301.
(16) Yang, C. X.; Cao, M. L.; Liu, H.; He, Y. Q.; Xu, J.; Du, Y.; Liu, Y. W.; Wang, W. J.; Cui, L.; Hu, J. J.; Gao, F. The High and Low Molecular Weight Forms of Hyaluronan Have Distinct Effects on CD44 Clustering. *J. Biol. Chem.* **2012**, *287* (51), 43094−43107.
(17) Slomiany, M. G.; Dai, L.; Tolliver, L. B.; Grass, G. D.; Zeng, Y. P.; Toole, B. P. Inhibition of Functional Hyaluronan-CD44 Interactions in CD133-positive Primary Human Ovarian Carcinoma Cells by Small Hyaluronan Oligosaccharides. *Clin. Cancer Res.* **2009**, *15* (24), 7593−7601.
(18) Toole, B. P.; Ghatak, S.; Misra, S. Hyaluronan Oligosaccharides as a Potential Anticancer Therapeutic. *Current Pharmaceutical Biotechnology* **2008**, *9* (4), 249−252.
(19) Urakawa, H.; Nishida, Y.; Knudson, W.; Knudson, C. B.; Arai, E.; Kozawa, E.; Futamura, N.; Wasa, J.; Ishiguro, N. Therapeutic Potential of Hyaluronan Oligosaccharides for Bone Metastasis of Breast Cancer. *Journal of Orthopaedic Research* **2012**, *30* (4), 662−672.
(20) Tolg, C.; McCarthy, J. B.; Yazdani, A.; Turley, E. A. Hyaluronan and RHAMM in Wound Repair and the ″Cancerization″ of Stromal Tissues. *Biomed Research International* **2014**, *2014*, 103923.
(21) Bourguignon, L. Y. W.; Wong, G.; Earle, C. A.; Xia, W. L. Interaction of Low Molecular Weight Hyaluronan with CD44 and Toll-Like Receptors Promotes the Actin Filament-Associated Protein 110-Actin Binding and MyD88-NF kappa B Signaling Leading to Proinflammatory Cytokine/Chemokine Production and Breast Tumor Invasion. *Cytoskeleton* **2011**, *68* (12), 671−693.
(22) Yu, Q.; Stamenkovic, I. Localization of Matrix Metalloproteinase 9 to the Cell Surface Provides a Mechanism for CD44-mediated Tumor Invasion. *Genes Dev.* **1999**, *13* (1), 35−48.
(23) Xu, X. M.; Chen, Y. X.; Chen, J. G.; Yang, S. M.; Gao, F.; Underhill, C. B.; Creswell, K.; Zhang, L. R. A Peptide with Three Hyaluronan Binding Motifs Inhibits Tumor Growth and Induces Apoptosis. *Cancer Res.* **2003**, *63* (18), 5685−5690.
(24) Song, G. L.; Liao, X. L.; Zhou, L.; Wu, L. H.; Feng, Y.; Han, Z. C. HI44a, an Anti-CD44 Monoclonal Antibody, Induces Differentiation and Apoptosis of Human Acute Myeloid Leukemia Cells. *Leukemia research* **2004**, *28* (10), 1089−1096.
(25) Jin, L. Q.; Hope, K. J.; Zhai, Q. L.; Smadja-Joffe, F.; Dick, J. E. Targeting of CD44 Eradicates Human Acute Myeloid Leukemic Stem Cells. *Nature medicine* **2006**, *12* (10), 1167−1174.
(26) Tremmel, M.; Matzke, A.; Albrecht, I.; Laib, A. M.; Olaku, V.; Ballmer-Hofer, K.; Christofori, G.; Heroult, M.; Augustin, H. G.; Ponta, H.; Orian-Rousseau, V. A CD44v6 Peptide Reveals a Role of CD44 in VEGFR-2 Signaling and Angiogenesis. *Blood* **2009**, *114* (25), 5236−5244.
(27) Matzke, A.; Herrlich, P.; Ponta, H.; Orian-Rousseau, W. A Five-Amino-Acid Peptide Blocks Met- and Ron-Dependent Cell Migration. *Cancer Res.* **2005**, *65* (14), 6105−6110.
(28) Khan, F.; Gurung, S.; Gunassekaran, G. R.; Vadevoo, S. M. P.; Chi, L. H.; Permpoon, U.; Haque, M. E.; Lee, Y. K.; Lee, S. W.; Kim, S.; Lee, B. Identification of Novel CD44v6-Binding Peptides that Block CD44v6 and Deliver a Pro-Apoptotic Peptide to Tumors to Inhibit Tumor Growth and Metastasis in Mice. *Theranostics* **2021**, *11* (3), 1326−1344.
(29) Peck, D.; Isacke, C. M. Hyaluronan-dependent Cell Migration Can be Blocked by a CD44 Cytoplasmic Domain Peptide Containing a Phosphoserine at Position 325. *Journal of cell science* **1998**, *111*, 1595−1601.
(30) Piotrowicz, R. S.; Damaj, B. B.; Hachicha, M.; Incardona, F.; Howell, S. B.; Finlayson, M. A6 Peptide Activates CD44 Adhesive Activity, Induces FAK and MEK Phosphorylation, and Inhibits the Migration and Metastasis of CD44-Expressing Cells. *Molecular cancer therapeutics* **2011**, *10* (11), 2072−2082.
(31) Misra, S.; Hascall, V. C.; De Giovanni, C.; Markwald, R. R.; Ghatak, S. Delivery of CD44 shRNA/Nanoparticles within Cancer Cells Perturbation of Hyaluronan/CD44v6 Interactions and Reduction in Adenoma Growth in Apc Min/ Plus Mice. *J. Biol. Chem.* **2009**, *284* (18), 12432−12446.
(32) Amorim, S.; Pashkuleva, I.; Reis, C. A.; Reis, R. L.; Pires, R. A. Tunable Layer-by-Layer Films Containing Hyaluronic Acid and Their Interactions with CD44. *J. Mater. Chem. B* **2020**, *8* (17), 3880−3885.
(33) Amorim, S.; da Costa, D. S.; Pashkuleva, I.; Reis, C. A.; Reis, R. L.; Pires, R. A. Hyaluronic Acid of Low Molecular Weight Triggers the Invasive ″Hummingbird″ Phenotype on Gastric Cancer Cells. *Adv. Biosyst* **2020**, *4* (11), 2000122.
(34) Amorim, S.; da Costa, D. S.; Mereiter, S.; Pashkuleva, I.; Reis, C. A.; Reis, R. L.; Pires, R. A. Multilayer Platform to Model the Bioactivity of Hyaluronic Acid in Gastric Cancer. *Mat Sci. Eng. C-Mater.* **2021**, *119*, 111616.
(35) Amorim, S.; da Costa, D. S.; Pashkuleva, I.; Reis, C. A.; Reis, R. L.; Pires, R. A. 3D Hydrogel Mimics of the Tumor Microenvironment: The Interplay Among Hyaluronic Acid, Stem Cells and Cancer Cells. *Biomater Sci-Uk* **2021**, *9* (1), 252−260.
(36) Beers, K. L.; Boo, S.; Gaynor, S. G.; Matyjaszewski, K. Atom Transfer Radical Polymerization of 2-Hydroxyethyl Methacrylate. *Macromolecules* **1999**, *32* (18), 5772−5776.
(37) Adharis, A.; Ketelaar, T.; Komarudin, A. G.; Loos, K. Synthesis and Self-Assembly of Double-Hydrophilic and Amphiphilic Block Glycopolymers. *Biomacromolecules* **2019**, *20* (3), 1325−1333.
(38) Gallow, K. C.; Jhon, Y. K.; Genzer, J.; Loo, Y. L. Influence of Gradient Strength and Composition Profile on the Onset of the Cloud Point Transition in Hydroxyethyl Methacrylate/Dimethylaminoethyl Methacrylate Gradient Copolymers. *Polymer* **2012**, *53* (5), 1131−1137.
(39) Han, Y.; Li, D. J.; Li, D. Q.; Chen, W. W.; Mu, S. E.; Chen, Y. Q.; Chai, J. L. Impact of Refractive Index Increment on the Determination of Molecular Weight of Hyaluronic Acid by Muti-Angle Laser Light-Scattering Technique. *Sci. Rep.* **2020**, *10* (1), 1858.
(40) Stern, R.; Jedrzejas, M. J. Hyaluronidases: Their Genomics, Structures, and Mechanisms of Action. *Chem. Rev.* **2006**, *106* (3), 818−839.
(41) Fang, S. P.; Putnam, A.; LaBarre, M. J. Kinetic Investigation of Recombinant Human Hyaluronidase PH20 on Hyaluronic Acid. *Anal. Biochem.* **2015**, *480*, 74−81.
(42) Schatz, C.; Lecommandoux, S. Polysaccharide-Containing Block Copolymers: Synthesis, Properties and Applications of an Emerging Family of Glycoconjugates. *Macromol. Rapid Commun.* **2010**, *31* (19), 1664−1684.
(43) Bonduelle, C.; Huang, J.; Ibarboure, E.; Heise, A.; Lecommandoux, S. Synthesis and Self-Assembly of ″Tree-Like″ Amphiphilic Glycopolypeptides. *Chem. Commun.* **2012**, *48* (67), 8353−8355.
(44) Duan, H. H.; Donovan, M.; Foucher, A.; Schultze, X.; Lecommandoux, S. Multivalent and Multifunctional Polysaccharide-Based Particles for Controlled Receptor Recognition. *Sci. Rep.* **2018**, *8*, 14730.
(45) Duan, H. H.; Donovan, M.; Hernandez, F.; Di Primo, C.; Garanger, E.; Schultze, X.; Lecommandoux, S. Hyaluronic-Acid-Presenting Self-Assembled Nanoparticles Transform a Hyaluronidase HYAL1 Substrate into an Efficient and Selective Inhibitor. *Angew. Chem., Int. Ed.* **2020**, *59* (32), 13591−13596.
(46) Kiessling, L. L.; Grim, J. C. Glycopolymer Probes of Signal Transduction. *Chem. Soc. Rev.* **2013**, *42* (10), 4476−4491.

https://doi.org/10.1021/acsami.2c11864
ACS Appl. Mater. Interfaces XXXX, XXX, XXX−XXX

(47) Collis, D. W. P.; Yilmaz, G.; Yuan, Y.; Monaco, A.; Ochbaum, G.; Shi, Y.; O'Malley, C.; Uzunova, V.; Napier, R.; Bitton, R.; Becer, C. R.; Azevedo, H. S. Hyaluronan (HA)-Inspired Glycopolymers as Molecular Tools for Studying HA Functions. *RSC Chemical Biology* **2021**, *2* (2), 568−576.
(48) Iyer, S.; Rele, S.; Grasa, G.; Nolan, S.; Chaikof, E. L. Synthesis of a Hyaluronan Neoglycopolymer by Ring-Opening Metathesis Polymerization. *Chem. Commun.* **2003**, No. 13, 1518−1519.
(49) Novoa-Carballal, R.; Carretero, A.; Pacheco, R.; Reis, R. L.; Pashkuleva, I. Star-Like Glycosaminoglycans with Superior Bioactivity Assemble with Proteins into Microfibers. *Chem.—Eur. J.* **2018**, *24* (54), 14341−14345.
(50) Calderón, M.; Quadir, M. A.; Sharma, S. K.; Haag, R. Dendritic Polyglycerols for Biomedical Applications. *Adv. Mater.* **2010**, *22* (2), 190−218.
(51) Montheard, J. P.; Chatzopoulos, M.; Chappard, D. 2-Hydroxyethyl Methacrylate (HEMA) - Chemical Properties and Applications in Biomedical Fields. *J. Macromol. Sci. R M C* **1992**, *C32* (1), 1−34.
(52) Zare, M.; Bigham, A.; Zare, M.; Luo, H.; Rezvani Ghomi, E.; Ramakrishna, S. pHEMA: An Overview for Biomedical Applications. *International Journal of Molecular Sciences* **2021**, *22* (12), 6376.
(53) Silva, C.; Carretero, A.; da Costa, D. S.; Reis, R. L.; Novoa-Carballal, R.; Pashkuleva, I. Design of Protein Delivery Systems by Mimicking Extracellular Mechanisms for Protection of Growth Factors. *Acta Biomaterialia* **2017**, *63*, 283−293.
(54) Antonietti, M.; Heinz, S.; Schmidt, M.; Rosenauer, C. Determination of the Micelle Architecture of Polystyrene Poly(4-Vinylpyridine) Block-Copolymers in Dilute-Solution. *Macromolecules* **1994**, *27* (12), 3276−3281.
(55) Esquenet, C.; Buhler, E. Aggregation Behavior in Semidilute Rigid and Semirigid Polysaccharide Solutions. *Macromolecules* **2002**, *35* (9), 3708−3716.
(56) Nehme, R.; Nasreddine, R.; Orlic, L.; Lopin-Bon, C.; Hamacek, J.; Piazza, F. Kinetic Theory of Hyaluronan Cleavage by Bovine Testicular Hyaluronidase in Standard and Crowded Environments. *Bba-Gen Subjects* **2021**, *1865* (3), 129837.
(57) Silva, C.; Novoa-Carballal, R.; Reis, R. L.; Pashkuleva, I. Following the Enzymatic Digestion of Chondroitin Sulfate by a Simple GPC Analysis. *Anal. Chim. Acta* **2015**, *885*, 207−213.
(58) Deschrevel, B.; Tranchepain, F.; Vincent, J. C. Chain-length Dependence of the Kinetics of the Hyaluronan Hydrolysis Catalyzed by Bovine Testicular Hyaluronidase. *Matrix Biology* **2008**, *27* (5), 475−486.
(59) Vercruysse, K. P.; Lauwers, A. R.; Demeester, J. M. Kinetic Investigation of The Degradation of Hyaluronan by Hyaluronidase Using Gel-Permeation Chromatography. *Journal of Chromatography B-Biomedical Applications* **1994**, *656* (1), 179−190.
(60) Fayad, S.; Nehme, R.; Langmajerova, M.; Ayela, B.; Colas, C.; Maunit, B.; Jacquinet, J. C.; Vibert, A.; Lopin-Bon, C.; Glatz, Z.; Morin, P. Hyaluronidase Reaction Kinetics Evaluated by Capillary Electrophoresis with UV and High-Resolution Mass Spectrometry (HRMS) Detection. *Anal. Chim. Acta* **2017**, *951*, 140−150.
(61) Todd, M. J.; Gomez, J. Enzyme Kinetics Determined Using Calorimetry: A General Assay for Enzyme Activity? *Anal. Biochem.* **2001**, *296* (2), 179−187.
(62) Wang, Y.; Wang, G. Y.; Moitessier, N.; Mittermaier, A. K. Enzyme Kinetics by Isothermal Titration Calorimetry: Allostery, Inhibition, and Dynamics. *Frontiers in Molecular Biosciences* **2020**, *7*, 583826.
(63) Valcarcel, J.; García, M. R.; Varela, U. R.; Vázquez, J. A. Hyaluronic Acid of Tailored Molecular Weight by Enzymatic and Acid Depolymerization. *Int. J. Biol. Macromol.* **2020**, *145*, 788−794.
(64) Cowman, M. K.; Matsuoka, S. Experimental Approaches to Hyaluronan Structure. *Carbohydr. Res.* **2005**, *340* (5), 791−809.
(65) Mizrahy, S.; Raz, S. R.; Hasgaard, M.; Liu, H.; Soffer-Tsur, N.; Cohen, K.; Dvash, R.; Landsman-Milo, D.; Bremer, M.; Moghimi, S. M.; Peer, D. Hyaluronan-Coated Nanoparticles: The Influence of the Molecular Weight on CD44-Hyaluronan Interactions and on the Immune Response. *J. Controlled Release* **2011**, *156* (2), 231−238.
(66) Ogino, S.; Nishida, N.; Umemoto, R.; Suzuki, M.; Takeda, M.; Terasawa, H.; Kitayama, J.; Matsumoto, M.; Hayasaka, H.; Miyasaka, M.; Shimada, I. Two-State Conformations in the Hyaluronan-Binding Domain Regulate CD44 Adhesiveness under Flow Condition. *Structure* **2010**, *18* (5), 649−656.
(67) Zwanzig, R. Two-State Models of Protein Folding Kinetics. *Proc. Natl. Acad. Sci. U.S.A.* **1997**, *94* (1), 148−150.
(68) Banerji, S.; Wright, A. J.; Noble, M.; Mahoney, D. J.; Campbell, I. D.; Day, A. J.; Jackson, D. G. Structures of the CD44-Hyaluronan Complex Provide Insight into a Fundamental Carbohydrate-Protein Interaction. *Nature Structural & Molecular Biology* **2007**, *14* (3), 234−239.
(69) Wolny, P. M.; Banerji, S.; Gounou, C.; Brisson, A. R.; Day, A. J.; Jackson, D. G.; Richter, R. P. Analysis of CD44-Hyaluronan Interactions in an Artificial Membrane System Insights into the Distinct Binding Properties of High and Low Molecular Weight Hyaluronan. *J. Biol. Chem.* **2010**, *285* (39), 30170−30180.
(70) Lesley, J.; Hascall, V. C.; Tammi, M.; Hyman, R. Hyaluronan Binding by Cell Surface CD44. *J. Biol. Chem.* **2000**, *275* (35), 26967−26975.
(71) Banerji, S.; Hide, B. R. S.; James, J. R.; Noble, M. E. M.; Jackson, D. G. Distinctive Properties of the Hyaluronan-binding Domain in the Lymphatic Endothelial Receptor Lyve-1 and Their Implications for Receptor Function. *J. Biol. Chem.* **2010**, *285* (14), 10724−10735.
(72) Carvalho, A. M.; Teixeira, R.; Novoa-Carballal, R.; Pires, R. A.; Reis, R. L.; Pashkuleva, I. Redox-Responsive Micellar Nanoparticles from Glycosaminoglycans for CD44 Targeted Drug Delivery. *Biomacromolecules* **2018**, *19* (7), 2991−2999.
(73) Sheridan, C.; Kishimoto, H.; Fuchs, R. K.; Mehrotra, S.; Bhat-Nakshatri, P.; Turner, C. H.; Goulet, R.; Badve, S.; Nakshatri, H. CD44(+)/CD24(−) Breast Cancer Cells Exhibit Enhanced Invasive Properties: An Early Step Necessary for Metastasis. *Breast Cancer Research* **2006**, *8* (5), R59.
(74) Li, W. Z.; Ma, H. L.; Zhang, J.; Zhu, L.; Wang, C.; Yang, Y. L. Unraveling the Roles of CD44/CD24 and ALDH1 as Cancer Stem Cell Markers in Tumorigenesis and Metastasis. *Sci. Rep.* **2017**, *7*, 13856.

https://doi.org/10.1021/acsami.2c11864
ACS Appl. Mater. Interfaces XXXX, XXX, XXX−XXX